FINITE VOLUME PERSPECTIVES ON FINITE DIFFERENCE SCHEMES AND BOUNDARY FORMULATIONS FOR WAVE SIMULATION

Brian Hamilton,[*]

Acoustics and Audio Group,
University of Edinburgh
brian.hamilton@ed.ac.uk

ABSTRACT

Time-domain finite difference (FD) and digital waveguide mesh (DWM) methods have seen extensive exploration as techniques for physical modelling sound synthesis and artificial reverberation. Various formulations of these methods have been unified under the FD framework, but many discrete boundary models important in room acoustics applications have not been. In this paper, the finite volume (FV) framework is used to unify various FD and DWM topologies, as well as associated boundary models. Additional geometric insights on existing stability conditions provide guidance into the FV meshing pre-processing step necessary for the acoustic modelling of irregular and realistic room geometries. DWM "1-D" boundary terminations are shown, through an equivalent FV formulation, to have a consistent multidimensional interpretation that is approximated to second-order accuracy, however the geometry and wall admittances being approximated may vary from what is desired. It is also shown that certain re-entrant corner configurations can lead to instabilities and an alternative stable update is provided for one problematic configuration.

1. INTRODUCTION

Finite difference (FD) methods applied to time-domain partial differential equations have a long history [1] and have, more recently, become popular techniques for wave simulation in musical acoustics and room acoustics modelling. FD methods have appeared in the acoustics literature in various forms, including the digital waveguide mesh (DWM) [2, 3], and the "finite difference time domain" (FDTD) [4, 5] and transmission line matrix (TLM) methods [6] adapted from electromagnetics [7, 8, 9]. The DWM and TLM methods were originally expressed in terms of scattering variables, but they are equivalent to FD methods when expressed solely in terms of nodal quantities [2, 8, 10].

Finite element (FE) methods comprise another major family of numerical methods that can be used for time-stepping wave simulations [11]. FE methods are based on unstructured grids of cells and interpolants defined over points within those cells. One advantage of FE methods over FD methods is that they are well-suited to irregular geometries (boundaries), whereas FD methods are suited to simple geometries, or "staircase" approximations to irregular boundaries. FE methods have been applied to musical acoustics problems [12], though generally not for sound synthesis.

Finite volume (FV) methods can be seen as a medium between these two methods [13], as they are based on grids of volumetric cells and differences between points within those cells. FV methods on Cartesian grids were introduced to room acoustics and shown to be equivalent to the Cartesian FDTD method [14, 4], but they have not seen the same popularity as the finite difference based methods. Recently, FV methods have been reintroduced for acoustical applications, but on unstructured grids and with rigorous energy-based stability analyses, allowing for the modelling of irregular geometries [15].

FV schemes can reduce to FD schemes on the interior domain when the tiling is regular, providing computationally efficient calculations appropriate for large domains such as in 3-D room acoustics modelling. This was shown for the Cartesian case and the 2-D hexagonal case [15] and later on the 3-D face-centered cubic (FCC) grid with rhombic dodecahedral cells [16]. Equivalences such as these remain to be determined for the rest of the DWM topologies. This is the first contribution of this study, which is presented in Section 4, after the introduction of the model equations and finite volume formulations in Sections 2 and 3. The second contribution of this study is a geometrical interpretation of passivity conditions at boundary cells (given certain constraints on the tiling), which provides insight towards meshing of irregular domains (Section 5). Various boundary models have been presented for FD/DWM methods [3, 17, 18], but their FV interpretations have yet to be determined. This is the third contribution of this study (Section 6). Conclusions and future work are given in Section 7.

2. MODEL EQUATIONS

2.1. Second-order wave equation

There have generally been two departure points for time-domain finite difference schemes in acoustics. The first is the second-order wave equation:

$$\partial_t^2 \Psi - c^2 \Delta \Psi = 0\,, \tag{1}$$

where $\Psi := \Psi(t, \mathbf{x})$ represents a velocity potential field, $t \in \mathbb{R}^+$ is time, $\mathbf{x}$ is a position vector within a d-dimensional closed volume $\mathcal{V} \subset \mathbb{R}^d$, Δ is the d-dimensional Laplacian operator, $\Delta := \sum_{i=1}^{d} \partial_{x_i}^2$, and c is the wave speed, assumed to be constant. The notation ∂_t denotes the partial derivative with respect to t, and similarly for spatial directions. The most common FD scheme for this equation was provided by Courant et al. [1], and the multidimensional extensions ($d \geq 3$) can be found in [19]. It was later applied to acoustic modelling for seismology [20], with Ψ as the variable of interest. Another wave equation can be found in the pressure field $p := p(t, \mathbf{x})$ through the use of the first of the two following relationships:

$$p = \rho \partial_t \Psi\,, \quad \mathbf{v} = -\nabla \Psi\,, \tag{2}$$

[*] This work was supported by the European Research Council, under grant StG-2011-279068-NESS, and by the Natural Sciences and Engineering Research Council of Canada.

where ρ represents the density of air and $\mathbf{v} := \mathbf{v}(t, \mathbf{x})$ is the particle velocity field. The pressure wave equation is then

$$\partial_t^2 p - c^2 \Delta p = 0\,. \tag{3}$$

Eqs. (1) and (3) are ultimately equivalent, but one must take care in choosing the appropriate source, boundary conditions, and output for (3) as it is one time-derivative higher than (1). FD methods were also applied to Eq. (3) for seismology [21], and later, DWM methods derived from networks of "acoustic tubes" were also expressed as FD schemes for this wave equation in 2-D [2] and in 3-D [3].

2.2. Conservation equations

The second departure point has been the following linear hyperbolic system, i.e. the conservation equations:

$$\frac{1}{\rho c^2}\partial_t p = -\nabla \cdot \mathbf{v} \qquad \text{(cons. of momentum)}\,, \tag{4a}$$

$$\rho \partial_t \mathbf{v} = -\nabla p \qquad \text{(cons. of mass)}\,, \tag{4b}$$

where $\nabla\cdot$ and ∇ are the d-dimensional divergence and gradient operators respectively. The FDTD[1] method, a popular technique for simulating Maxwell's equations on staggered grids, was adapted to the acoustics equations (4a) and (4b) for the purposes of vocal tract simulation [5] and room acoustics modelling [4]. These equations were also approached using TLM methods adapted from electromagnetics [6], and FV methods [14]. It is straightforward to check that these are different forms for the same underlying system, i.e. (4a) and (4b) give (3), and (1) is recovered using (2). Similarly, it has been shown that the various discretised forms (FD, DWM, TLM, FDTD, FV) are equivalent when implemented on Cartesian grids [24, 23, 2, 3, 10, 22, 15].

3. FINITE VOLUME APPROXIMATION

3.1. Cells and tiling

The following describes a general notation for a tiling of the volume $\mathcal{V}$ by cells in d-dimensions, which will be used to derive a finite volume approximation for the model equations. A tiling of $\mathcal{V}$ is made up of closed cells $\mathcal{C}_i$ indexed by $i \in I$, whose interiors are pairwise disjoint, i.e. $\bigcup_{i\in I} \mathcal{C}_i = \mathcal{V}$, and the boundary of each cell is denoted by $\partial\mathcal{C}_i$. A $(d-1)$-dimensional face (or side) of the cell $\mathcal{C}_i$ is denoted by $\mathcal{S}_{ij} := \mathcal{C}_i \cap \mathcal{C}_j = \mathcal{S}_{ji}$ and its $(d-1)$-dimensional volume is S_{ij}. Any cell $\mathcal{C}_j$ such that $\mathcal{S}_{ij} \neq \{\}$ is a neighbouring cell of $\mathcal{C}_i$. Let N_i be the index set of the neighbouring cells of $\mathcal{C}_i$ and let $K_i := |N_i|$, where $|N_i|$ denotes the cardinality of the set. A boundary face is denoted by $\mathcal{S}_{i(b)} := \mathcal{C}_i \cap \partial\mathcal{V}$ and its $(d-1)$-dimensional volume is denoted by $S_{i(b)}$. Finally, let $I_{(i)}$ and $I_{(b)}$ represent the index sets where $S_{i(b)} = 0$ and $S_{i(b)} > 0$ respectively. Note, in 1-D cell-faces are just points, so it suffices to set all measures $S_{ij} = 1$ when $\mathcal{S}_{ij} \neq \{\}$ and likewise, $S_{i(b)} = 1$ when $\mathcal{S}_{i(b)} \neq \{\}$ for the case $d = 1$. The tiling will also have an associated grid of points $\mathbb{G} := \{\mathbf{x}_i \in \mathcal{V}, i \in I\}$ such that $\mathbf{x}_i$ is not a point shared with other cells, i.e. $\mathbf{x}_i \in \mathcal{C}_i \setminus (\bigcup_{j\in N_i} \mathcal{S}_{ij})$.

[1] In this study, the acronym "FDTD" will refer only to staggered schemes for the system (4) which were adapted from the electromagnetics literature [7, 9]. Second-order wave equation schemes, which are much older [1], are more commonly (and efficiently [22]) employed will simply be called "FD methods" to be more consistent with the larger body of literature on numerical methods for such equations [1, 19, 23] and their applications in various fields [24, 20, 21]. The additional "time-domain" distinction is not necessary here, since this is implied by the model equations.

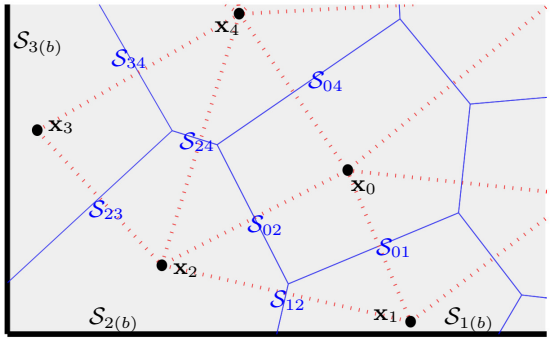

Figure 1: A section of a 2-D tiling, and the triangulation of its grid of points $\mathbb{G}$. The interior is shaded and part of the boundary $\partial\mathcal{V}$ is denoted by the thick line.

For the purposes of this paper, it will be assumed that $\mathcal{C}_i$ is the Voronoi cell of $\mathbf{x}_i$ for $i \in I_{(i)}$ and it will be further assumed that the line segment with endpoints $\mathbf{x}_i$ and $\mathbf{x}_j$ (denoted by $\overline{\mathbf{x}_i\mathbf{x}_j}$) for $j \in N_i$ is oriented normal to $\mathcal{S}_{ij}$ and passes through that side. Not all Voronoi tessellations have this "line of sight" property; those that do are the dual tilings of *Pitteway triangulations* (of $\mathbb{G}$) [25]. Such a tiling is illustrated in Fig. 1.

3.2. Integral form

A finite volume formulation can be derived starting from the acoustic velocity potential wave equation and integrating over the volumetric cell $\mathcal{C}_i$,

$$\int_{\mathcal{C}_i} \partial_t^2 \Psi \, dV = c^2 \int_{\mathcal{C}_i} \Delta\Psi \, dV\,. \tag{5}$$

Using $\Delta\Psi = \nabla\cdot\nabla\Psi$ and the divergence theorem gives

$$\int_{\mathcal{C}_i} \partial_t^2 \Psi \, dV = c^2 \int_{\partial\mathcal{C}_i} \mathbf{n}\cdot\nabla\Psi \, d\sigma\,, \tag{6}$$

where $\mathbf{n}$ denotes the outward normal vector at $\mathbf{x} \in \partial\mathcal{C}_i$. Then using $\partial\mathcal{C}_i = (\bigcup_j \mathcal{S}_{ij}) \cup \mathcal{S}_{i(b)}$, (6) can be written as

$$\int_{\mathcal{C}_i} \partial_t^2 \Psi \, d\mathbf{x} = c^2 \sum_{j\in N_i} \int_{\mathcal{S}_{ij}} \mathbf{n}\cdot\nabla\Psi \, d\sigma - c^2 \int_{\mathcal{S}_{i(b)}} \mathbf{n}\cdot\mathbf{v} \, d\sigma\,. \tag{7}$$

The last term isolates the velocity field pointing out of the boundary, which can be used to implement impedance boundary conditions.

3.3. Finite volume schemes

Let $\hat{\Psi} = \hat{\Psi}(t, \mathbf{x})$ represent an approximation to the acoustic velocity potential $\Psi(t, \mathbf{x})$, and the following abbreviated notation will be used: $\hat{\Psi}_i^{\pm} := \hat{\Psi}(t \pm k, \mathbf{x}_i)$ for some time-step k. The difference operators that will provide a discrete approximation to (7) are

Table 1: Isohedral cells and FD/DWM/FDTD equivalents (found in the literature) for pointwise FV approximations

cell ($\mathcal{C}_i$)	dim. (d)	K_i	$\frac{2d}{K_i}$	$\delta_\Delta = \Delta + O(h^q)$	grid	FD/DWM scheme	staggered (FDTD) scheme for (4)
line segment	1	2	1	$q=2$	integer lattice	standard FD scheme [1]	[24, 23]
regular triangle	2	3	4/3	$q=1$	honeycomb grid	"hexagonal DWM" [26]	-
square	2	4	1	$q=2$	square grid	standard FD scheme [1]	Yee's 2-D scheme (FDTD) [7]*
hexagon	2	6	2/3	$q=2$	hexagonal grid	hexagonal FD scheme [27]	hexagonal FDTD [28]*
cube	3	6	1	$q=2$	cubic grid	standard FD scheme [19]	Cartesian FDTD [4, 5]
regular tetrahedron†	3	4	3/2	$q=1$	diamond grid	"tetrahedral DWM" [26]	-
octahedron†	3	8	3/4	$q=2$	BCC grid	"octahedral FD" scheme [10]	-
rhombic dodecahedron	3	12	1/2	$q=2$	FCC grid	"dodecahedral DWM" [29]	-

† does not tile space * see Footnote 2

defined as follows

$$\delta_{t\pm}\hat{\Psi}_i := \pm\frac{1}{k}(\hat{\Psi}_i^{\pm} - \hat{\Psi}_i)\,, \tag{8a}$$

$$\delta_{tt} := \delta_{t+}\delta_{t-} = \delta_{t-}\delta_{t+}\,, \tag{8b}$$

$$\delta_{ij}\hat{\Psi}_i := \frac{1}{h_{ij}}(\hat{\Psi}_j - \hat{\Psi}_i) = -\delta_{ji}\hat{\Psi}_i\,, \tag{8c}$$

where $h_{ij} = \|\mathbf{x}_{ij}\|$ and $\mathbf{x}_{ij} := \mathbf{x}_j - \mathbf{x}_i$.

Eq. (7) can be approximated by replacing Ψ with $\hat{\Psi}$ and then applying difference operators in the place of continuous derivatives. It must also be assumed that the approximation $\hat{\Psi}$ is constant (averaged) over cells and boundary sides [15]. This results in the following

$$\frac{V_i}{c^2}\delta_{tt}\hat{\Psi}_i = \sum_{j\in N_i} S_{ij}\delta_{ij}\hat{\Psi}_i - S_{i(b)}\hat{v}_{i(b)}\,, \tag{9}$$

where $\hat{v}_{i(b)}$ represents the boundary term averaged over $\mathcal{S}_{i(b)}$, to be specified by the boundary conditions. Due to the imposed restrictions on the Voronoi tessellation, $\delta_{ij}\hat{\Psi}_i$ can be seen as a centered difference about some point on the face $\mathcal{S}_{ij}$, and the approximation will be second-order accurate.

A finite volume approximation of the conservation equations can also be recovered by defining approximations to the pressure and velocity field, denoted by $\hat{p}$ and $\hat{\mathbf{v}}$ respectively, on staggered grids in space and time. Consider the following spatial and temporal half-step shift operators, applied to some function $u(t, \mathbf{x})$:

$$e_{t\pm}u_i := u(t \pm k/2, \mathbf{x}_i)\,, \tag{10a}$$

$$e_{ij\pm}u_i := u(t, \mathbf{x}_i \pm \mathbf{x}_{ij}/2) = e_{ji\mp}u_i\,. \tag{10b}$$

The pressure and velocity approximations are then staggered as

$$\hat{p}_i := e_{t-}\hat{p}(t, \mathbf{x}_i)\,, \tag{11a}$$

$$\hat{v}_{ij} := \mathbf{x}_{ij}\cdot e_{ij+}\hat{\mathbf{v}}(t, \mathbf{x}_i)\,, \tag{11b}$$

and these are related to $\hat{\Psi}_i$ using

$$\hat{p}_i = \rho\delta_{t-}\hat{\Psi}_i\,, \tag{12a}$$

$$\hat{v}_{ij} = -\delta_{ij}\hat{\Psi}_i\,, \tag{12b}$$

resulting in the equivalent (to (9)) staggered scheme:

$$\frac{V_i}{\rho c^2}\delta_{t+}\hat{p}_i = -\sum_{j\in N_i} S_{ij}\hat{v}_{ij} - S_{i(b)}\hat{v}_{i(b)}\,, \tag{13a}$$

$$\rho\delta_{t-}\hat{v}_{ij} = -\delta_{ij}\hat{p}_i\,. \tag{13b}$$

When $\mathcal{C}_i$ is a hexahedron, that is, the Voronoi cell of a "quasi-Cartesian" grid ($d = 3$), (13) defines the FV scheme proposed in [14]. The FV framework presented in [15] generalises these FV schemes to unstructured grids of polytopes ($d \geq 1$).

Finally, by applying $\rho\delta_{t-}$ to both sides of (13a) and substituting in (13b), or simply by applying (12a) to (9), a wave equation scheme for the pressure can be recovered, with an isolated boundary term:

$$\frac{V_i}{c^2}\delta_{tt}\hat{p}_i = \sum_{j\in N_i} S_{ij}\delta_{ij}\hat{p}_i - \rho S_{i(b)}\delta_{t-}\hat{v}_{i(b)}\,. \tag{14}$$

4. EQUIVALENCES WITH FD/DWM/FDTD SCHEMES

4.1. Pyramidal decomposition

In this section, only the interior cells will be considered ($i \in I_{(i)}$), so $\mathcal{S}_{i(b)} = \{\}$, or $S_{i(b)} = 0$. Taking into account the previously imposed restrictions ("line of sight"), an interior cell can then be divided into K_i d-dimensional pyramids $\mathcal{P}_{ij}$ with bases $\mathcal{S}_{ij}$, heights $h_{ij}/2$, and a shared apex $\mathbf{x}_i$. As is commonly known, the area of a 2-D pyramid (a triangle) is the area of the base times the height divided by two. This extends to d-dimensions [30], giving

$$V_i = \sum_{j\in N_i} V_{ij}\,, \quad V_{ij} := S_{ij}h_{ij}/(2d)\,. \tag{15}$$

A cell $\mathcal{C}_i$ will be called "isohedral" (face-transitive) when the parameters S_{ij} and h_{ij} are constants ($S_{ij} = S_i$, $h_{ij} = h_i$ for $j \in N_i$). The volume of an isohedral cell is then simply

$$V_i = K_i S_i h_i/(2d)\,. \tag{16}$$

This pyramidal decomposition is illustrated in Fig. 2 for square and hexagonal cells ($d = 2$), and various isohedral cells are listed in Table 1 for $d \in \{1, 2, 3\}$.

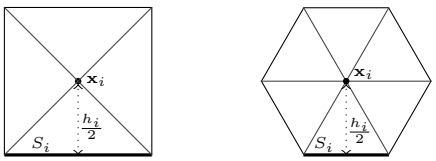

Figure 2: Square and hexagonal cells divided into pyramids. S_i denoted by thick line, $h_i/2$ denoted by dotted line.

4.2. Discrete Laplacians and wave equation FD/DWM schemes

Various FV schemes can be simplified using the pyramidal decomposition. The wave equation scheme in (14), for the isohedral cells

listed in Table 1, can be written as

$$\delta_{tt}\hat{p}_i = c^2\delta_\Delta\hat{p}_i\,, \quad \delta_\Delta\hat{p}_i := \frac{2d}{K_i h_i^2}\sum_{j\in N_i}(\hat{p}_j - \hat{p}_i) = \Delta\hat{p}_i + O(h^q)\,. \tag{17}$$

The spatial operator δ_Δ represents a discrete Laplacian with first ($q = 1$) or second-order ($q = 2$) accuracy, and (17) represents one of the various FD/DWM schemes that have appeared in the literature, as summarised in Table 1. Note, the regular tetrahedron and the octahedron do not tile space so they do not permit a full finite-volume approximation over $\mathcal{V}$. Nevertheless, the FD schemes derived from their single cell approximations are equivalent to the pointwise approximations from their associated FD/DWM schemes.

4.3. Discrete divergence and FDTD staggered schemes

Staggered (FDTD) schemes that employ isohedral cells can also be recovered from FV schemes. Using the pyramidal decomposition, (13a) becomes

$$\frac{1}{\rho c^2}\delta_{t+}\hat{p}_i = -\delta_{\nabla\cdot}\hat{\mathbf{v}}_i\,, \quad \delta_{\nabla\cdot}\hat{\mathbf{v}}_i := \frac{2d}{K_i h_i}\sum_{j\in N_i}\hat{v}_{ij} \tag{18}$$

The spatial operator $\delta_{\nabla\cdot}$ is essentially a discrete divergence operator, but this is more clear in the following special case. When the cell $\mathcal{C}_i$ is made up of pairs of parallel faces (K_i is even), the set N_i can be divided into two non-overlapping complementary sets $N_{i,1}$ and $N_{i,2}$ each with $K_i/2$ elements such that for every $j \in N_{i,1}$ there is a complementary index $j^* \in N_{i,2}$ where $\mathbf{x}_{ij} = -\mathbf{x}_{ij^*}$. Making use of the skew-symmetry $\hat{v}_{ij} = -\hat{v}_{ji}$ results in

$$\delta_{\nabla\cdot}\hat{\mathbf{v}}_i = \frac{2d}{K_i}\sum_{j\in N_{i,1}}\frac{1}{h_i}(e_{ij+} - e_{ij-})(\mathbf{x}_{ij}\cdot\hat{\mathbf{v}}_i) \approx \nabla\cdot\hat{\mathbf{v}}_i\,, \tag{19}$$

which is, more clearly, a sum of centered spatial differences in the directions of $\mathbf{x}_{ij}$ for $j \in N_{i,1}$. This defines the discrete divergence used in the Cartesian case ($\mathbf{x}_{ij}$ for $j \in N_{i,1}$ become the standard unit vectors in $\mathbb{R}^d$), leading to the staggered schemes adapted from Yee's scheme for Maxwell's equations [5, 4]. Furthermore, (18) leads to a hexagonal staggered scheme for acoustics similar in principle to one derived for Maxwell's equations [28].[2] In 3-D this leads to staggered schemes on the face-centered cubic (FCC) and body-centered cubic (BCC) grids. These equivalences are also summarised in Table 1. Clearly, these staggered schemes are all equivalent to their second-order wave equation counterparts, which generalises the link that has been established in the Cartesian case [22]. The staggered FDTD formulation is known to be less efficient than the wave equation formulation in the Cartesian case [22], and this can be shown for the non-Cartesian FDTD extensions for acoustics (left out for brevity). Wave equation schemes are also more efficient than their DWM forms in $d > 1$ [10].

5. STABILITY/PASSIVITY CONDITIONS

In this section, additional geometric insights will be provided on the stability conditions derived in [15], but the full energy analysis provided in [15] will be omitted for brevity. First, consider the lossless case, where the boundary velocity is set to zero,

[2] Maxwell's equations in polarised form (2-D) can be adapted to the acoustics equations (4) with a simple change of variables [31]. It is straightforward to show that this also applies to the 2-D FDTD schemes.

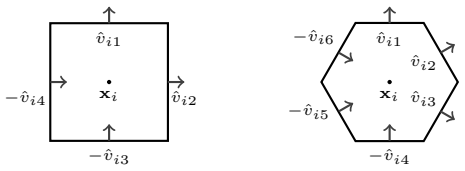

Figure 3: Square and hexagonal cells for staggered grid (FDTD) schemes

i.e. $\hat{v}_{i(b)} = 0$, $i \in I_{(b)}$. In the lossless case it can be shown that the total numerical energy remains bounded (stability) when the following condition is satisfied for each cell ($i \in I$) [15]:

$$k^2 \le \frac{2V_i}{c^2\sum_{j\in N_i} S_{ij}/h_{ij}}\,. \tag{20}$$

This appears to be the condition derived in [4] (considering only quasi-Cartesian grids) but, in fact, it is different. The condition derived in [4] does not distinguish between interior sides $\mathcal{S}_{ij}$ and boundary sides $\mathcal{S}_{i(b)}$, whereas the boundary sides are not counted in the denominator of (20). As such, condition (20) becomes more relaxed at the boundaries for Cartesian cells. The importance of this detail will be pointed out in Section 6.2.

5.1. A sufficient condition for interior isohedral cells

Further insight on condition (20) can be obtained when it is assumed that a "locally irregular" tiling is used, which means that the cells are isohedral and congruent when $i \in I_{(i)}$, but they may vary for $i \in I_{(b)}$. Thus, $K_i = K$, $S_{ij} = S$, $h_{ij} = h$, and $V_i = V$ for $i \in I_{(i)}$. For an interior cell ($i \in I_{(i)}$) the stability condition then becomes

$$k^2 \le \frac{2V}{c^2 K(S/h)}\,. \tag{21}$$

Using $V = KSh/(2d)$, the above reduces to

$$k^2 \le h^2/(c^2 d)\,, \tag{22}$$

or more simply, $\lambda \le \sqrt{1/d}$ where $\lambda := ck/h$ is the Courant number. This can be recognised as the condition obtained from von Neumann analysis for many schemes, including the Cartesian one [19]. In certain cases the von Neumann bound is more relaxed, such as in the hexagonal [10] and FCC schemes [16], as well as many parameterised schemes [10]. It is perhaps more appropriate to call (22) the "passivity condition" [10], since it implies that a DWM/TLM network implementation made up of concretely passive elements is possible, from which stability follows [32].

5.2. A sufficient condition for boundary cells

Now condition (20) will be simplified for boundary cells ($i \in I_{(b)}$). It will be assumed that $h_{ij} = h$, which implies that $\mathcal{C}_i$ has been cut or enlarged, but the point $\mathbf{x}_i$ has not moved from its regular position (for $i \in I_{(b)}$). It is straightforward to prove that $\lambda = \sqrt{1/d}$ is sufficient for stability at boundary cells that are congruent to interior cells (e.g., "staircase boundaries"); the denominator in (20) decreases but the total volume V_i does not, so the local condition at the boundary cell is more relaxed than $\lambda \le \sqrt{1/d}$.

Next, consider the case where the boundary cells are not congruent to the interior cells, which amounts to special cases of "fitted boundaries". Removing the volumes of the interior pyramids $\mathcal{P}_{ij}$

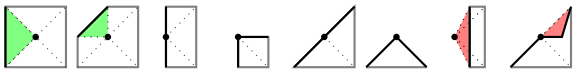

Figure 4: Some boundary cell types possible for a locally irregular square tiling. Green denotes positive V_i^*, red denotes negative V_i^*. Black line denotes $\mathcal{S}_{i(b)}$. Dotted lines denote pyramid divisions. (a)-(f) are stable with $\lambda = \sqrt{1/2}$, (g) and (h) are not.

from the volume of the cell $\mathcal{C}_i$ leaves a quantity denoted by V_i^*,

$$V_i^* := V_i - \sum_{j \in N_i} S_{ij} h/(2d)\,. \tag{23}$$

Then starting from (20), a bound on k^2 is

$$k^2 \leq \frac{2V_i}{c^2 \sum_{j\in N_i} S_{ij}/h} \leq \frac{\sum_{j\in N_i} S_{ij} h + V_i^*}{c^2 d \sum_{j\in N_i} S_{ij}/h} \tag{24a}$$

$$\leq h^2/(c^2 d) \quad \text{when } V_i^* \geq 0\,. \tag{24b}$$

Thus, $\lambda = \sqrt{1/d}$ is sufficient as long as $V_i^* \geq 0$. This condition is illustrated in Fig. 4 with some example 2-D cells in a locally irregular square tiling. Figs. 4g and 4h illustrate the types of cells that should be avoided since they will enforce more strict stability conditions than what is obtained from interior cells. This can be detrimental in audio applications as it reduces the overall temporal bandwidth of the output [33] and reduces the efficiency in minimising dispersion error [34].

It is worth pointing out a link with "conformal methods" for irregular boundary modelling in acoustical FDTD simulations [35, 36, 37]. These techniques are, ultimately, staggered schemes on locally irregular Cartesian grids, and more specifically, the "fitted boundaries" considered here. It was empirically found that a certain minimum volume had to be kept for locally conforming boundary cells, otherwise instabilities would be experienced [35, 36, 37], but a stability condition was not obtained. The condition that needs to be satisfied in such conformal methods is indeed the geometric one described here ($V_i^* \geq 0$), or more generally, condition (20).

6. BOUNDARY MODELS

Some commonly used discrete boundary models in FD/DWM methods can be shown to have equivalent FV formulations. To be considered are the simplest frequency independent lossy boundary conditions:

$$\mathbf{n} \cdot \mathbf{v} = (\gamma/\rho c) p\,, \quad \mathbf{x} \in \partial\mathcal{V}\,. \tag{25}$$

where $\gamma \geq 0$ represents the specific acoustic admittance. Applying one temporal derivative and employing (4b) gives the pressure boundary condition

$$-\,\mathbf{n} \cdot \nabla p = (\gamma/c)\partial_t p\,. \tag{26}$$

Frequency-independent lossy boundaries are achieved in the FV framework by discretising (25), while (26) has been the preferred condition in FD-based studies [38, 18, 33]. It will be seen that the FV and FD discretisations are essentially the same. To this end, the following average and difference operators will be necessary:

$$\mu_{t+}\hat{p}_i = \frac{1}{2}(\hat{p}_i^+ + \hat{p}_i)\,, \qquad \delta_{t\cdot}\hat{p}_i = \frac{1}{2k}(\hat{p}_i^+ - \hat{p}_i^-)\,. \tag{27}$$

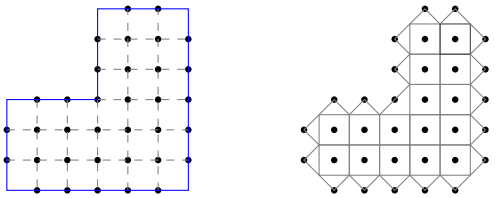

(a) DWM modelling (b) FV equivalent

Figure 5: Desired L-shaped domain in blue, modelled using 1-D DWM boundaries (left) and equivalent FV interpretation (right). Dashed lines indicate connectivity, or DWM delay lines. Notice that adjacent boundary nodes are not interconnected, in both cases.

In the FV formulation from [15], (25) is discretised on $\mathcal{S}_{i(b)}$ with

$$\hat{v}_{i(b)} = (\gamma/\rho c)\mu_{t+}\hat{p}_i\,. \tag{28}$$

Applying $\rho\delta_{t-}$ and using the identity $\delta_{t\cdot} = \mu_{t+}\delta_{t-}$ gives

$$\rho\delta_{t-}\hat{v}_{i(b)} = (\gamma/c)\delta_{t\cdot}\hat{p}_i\,, \tag{29}$$

and now defining a fictitious "ghost point" $\mathbf{x}_g := \mathbf{x}_i + \mathbf{n}/2$ outside of the domain (as employed in the FD framework, but unnecessary in the FV framework), one could write (29) as

$$-\,\delta_{ig}\hat{p}_i = (\gamma/c)\delta_{t\cdot}\hat{p}_i\,, \tag{30}$$

which is a (centered) FD discretisation of (26). This is just a starting point for equivalences between FV boundaries and FD boundaries. Still to consider are specific boundary geometries and boundary cell types.

It can be shown that as long as the interior energy remains bounded, the only extra condition for stability is $\gamma \geq 0$ (passivity) [15]. In other words, if the lossless case is stable then the lossy boundaries will remain stable. Thus, when $\gamma \geq 0$, the stability of the scheme is ensured with $\lambda \leq \sqrt{1/d}$ as long as $V_i^* \geq 0$ for $i \in I_{(b)}$.

6.1. DWM "1-D boundaries"

Using the DWM paradigm, boundaries in $d > 1$ are set via 1-D connections from boundary nodes to interior nodes. This is somewhat of an ambiguous way to set the boundaries, but it has the advantage of ensuring stability by virtue of a concretely passive network. For convenience, the DWM boundary node update, connected to K_i interior nodes, will be expressed in the FD equivalent formulation (the so-called "Kirchoff DWM"). Adapted from [17], the update is

$$(\gamma' + K_i)\hat{p}_i^+ = 2\sum_{j\in N_i} \hat{p}_j + (\gamma' - K_i)\hat{p}_i^-\,, \quad i \in I_{(b)}\,, \tag{31}$$

where γ' is meant to represent the desired γ in (26), but its precise value is to be determined. Dividing (31) through by K_i gives

$$\left((\gamma'/K_i) + 1\right)\hat{p}_i^+ = (2/K_i)\sum_{j\in N_i} \hat{p}_j + \left((\gamma'/K_i) - 1\right)\hat{p}_i^-\,. \tag{32}$$

The Courant number is set to $\lambda = \sqrt{1/d}$ for a DWM (by construction). In order to obtain the familiar DWM cancellation of the $\hat{p}_i$ term that would have appeared in the summation (see (17)) with the term $2\hat{p}_i$ left over from the expansion of $\delta_{tt}\hat{p}_i$, the following

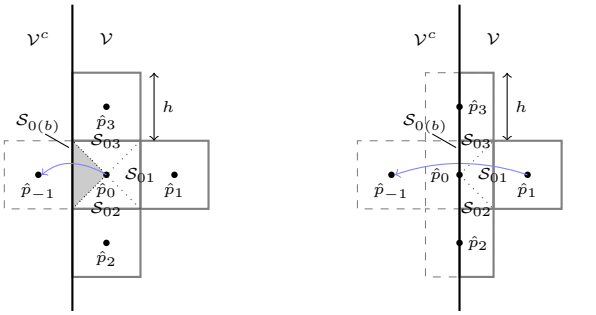

(a) Backwards difference (b) Centered difference

Figure 6: Backwards and centered spatial differences, in terms of FV cells. Dotted lines show pyramidal decomposition of $\mathcal{C}_0$. Volume pertaining to V_0^* is shaded. $\mathcal{V}^c$ denotes the exterior.

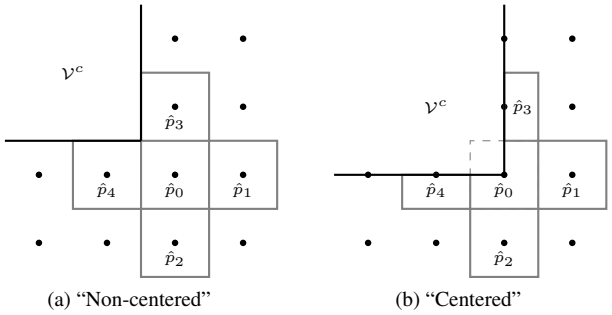

(a) "Non-centered" (b) "Centered"

Figure 7: Re-entrant corner configurations in 2-D with Cartesian grid

condition would be required from an equivalent FV formulation:

$$\lambda^2 K_i \frac{Sh}{V_i} = 2 \qquad \Rightarrow \qquad V_i = K_i \frac{Sh}{2d} \tag{33}$$

Thus, an equivalent, and multidimensionally consistent to second-order accuracy, FV interpretation of the DWM boundary cell is the union of K_i pyramids $\mathcal{P}_{ij}$ with a shared apex $\mathbf{x}_i$, bases $\mathcal{S}_{ij}$ (with $S_{ij} = S$) and heights $h/2$. This is illustrated in Fig. 5 for the Cartesian DWM on an L-shaped geometry. Note that the pyramidal boundary cells result in a crude approximation to the desired domain. Also note, the so-called "1-D ambiguity" problem [18] was avoided here, which is to interpret the Courant number as being set to unity locally at the boundary. It was suggested that this may lead to stability issues [38], but the DWM boundary model remains passive since it will always be the case that $V_i^* = 0$.

Finally, the precise value of γ' is found to be

$$\gamma' = \gamma \sqrt{d} (S_{i(b)}/S) \,. \tag{34}$$

Thus, γ' is not necessarily the desired acoustic admittance γ. It is consistent with γ in at least two special cases: $d = 1$ (as expected) and when $\gamma = 0$. For the boundary cells depicted in Fig. 5 one has $\gamma' = 2\gamma$. It should be pointed out that, while only the 2-D Cartesian case was illustrated, this FV interpretation extends to all other multidimensional DWM topologies, as long as the associated isohedral cell tiles d-dimensional space, which excludes the tetrahedral DWM and the octahedral DWM.

6.2. Centered and non-centered boundaries

Here, the basic 2-D FD scheme for the wave equation, also known as "standard leapfrog" (SLF), will be used to give an interpretation of boundaries commonly implemented for a half-plane. Consider the half-plane terminations featured in Fig. 6. Based on these two configurations, the spatial derivative in (26) can be approximated using one of the following spatial differences:

$$\frac{1}{h}(\hat{p}_0 - \hat{p}_{-1}) \approx -\mathbf{n}\cdot\nabla\hat{p}_0 \,, \qquad \frac{1}{2h}(\hat{p}_1 - \hat{p}_{-1}) \approx -\mathbf{n}\cdot\nabla\hat{p}_0 \,. \tag{35}$$

The former is a backwards "non-centered" difference and the latter is a centered difference. The centered difference has been preferred in the literature because it is, at first glance, second-order accurate [18]. However, the first operator is also centered if one redefines the boundary to lie between $\mathbf{x}_0$ and $\mathbf{x}_{-1}$, as in Fig. 6a. The temporal derivative (26) is usually approximated by $\delta_{t\cdot}$ to give an overall second-order accuracy. From the FD perspective, the update at the boundary node $\hat{p}_0$ is then:

$$\hat{p}_0^+ = \lambda^2(\hat{p}_{-1} + \hat{p}_1 + \hat{p}_2 + \hat{p}_3 - 4\hat{p}_0) + 2\hat{p}_0 - \hat{p}_0^- \,, \tag{36}$$

where $\hat{p}_{-1}$ represents the "ghost node" to be eliminated using the discretised boundary conditions. After eliminating the ghost node, the boundary update using the backwards spatial difference is

$$\hat{p}_0^+ = \frac{1}{1 + \frac{\gamma\lambda}{2}} \left(\lambda^2(\hat{p}_1 + \hat{p}_2 + \hat{p}_3 - 3\hat{p}_0) + 2\hat{p}_0 + \left(\frac{\gamma\lambda}{2} - 1 \right) \hat{p}_0^- \right) \,, \tag{37}$$

and the boundary update using the centered spatial difference is

$$\hat{p}_0^+ = \frac{1}{1 + \gamma\lambda} \left(\lambda^2(2\hat{p}_1 + \hat{p}_2 + \hat{p}_3 - 4\hat{p}_0) + 2\hat{p}_0 + (\gamma\lambda - 1)\, \hat{p}_0^- \right) \,. \tag{38}$$

On the other hand, both cases are summarised by the FV update:

$$\hat{p}_0^+ = \frac{1}{1 + \gamma\sigma} \left(\frac{c^2 k^2}{V_0 h} \sum_{j=1}^{3} S_{0j}(\hat{p}_j - \hat{p}_0) + 2\hat{p}_0 + (\gamma\sigma - 1)\, \hat{p}_0^- \right) , \tag{39}$$

where $\sigma := ckS_{0(b)}/(2V_0)$. For the full cell, one has $S_{0(b)} = S_{0j} = h$ for $j \in \{1, 2, 3\}$ and $V_0 = h^2$. Thus $\sigma = \lambda/2$ and the "backwards" update (37) is obtained ($c^2k^2S_{0j}/(V_0 h) = \lambda^2$). For the half cell, one has $S_{0(b)} = S_{01} = h$ and $S_{02} = S_{03} = h/2$, meanwhile $V_0 = h^2/2$, so $\sigma = \lambda$ and the "centered update" (38) is obtained.

In terms of stability, the full-cell has $V_0^* = h^2/4$ remaining after subtracting interior pyramids (seen in Fig. 6a), and the half-cell has $V_0^* = 0$. Thus, both conditions remain stable with $\lambda = \sqrt{1/2}$, which is consistent with the literature [18, 33]. On the other hand, using the stability condition derived in [14] one would obtain a restriction of $\lambda \leq \sqrt{1/3}$ at the half-cell, which is too strict.

It is straightforward to extend this type of analysis to the corner case in 2-D (quarter-cell, Fig. 4d) and further, to wall, edge, corner FD conditions with cubic cells in 3-D [18]. These turn out to be cubic cells that are cut into one-half, one-quarter, and one-eighth respectively.

6.3. Re-entrant corners

Re-entrant corners are simple examples of irregular geometries to be modelled. An example re-entrant corner is displayed in Fig. 7, in two different configurations with respect to a square grid. In

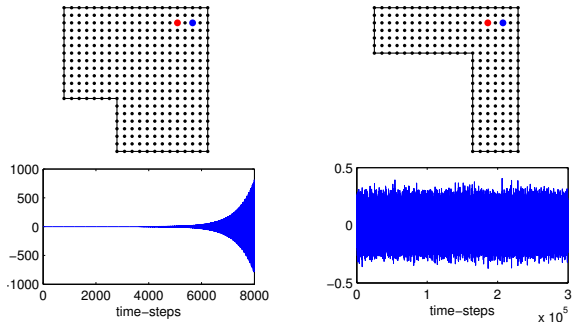

(a) Domain A (b) Domain B

Figure 8: Top: two test domains. The scheme is initialised by setting $\hat{p}$ to zero at $t = 0$, and $\hat{p}$ is set to -1 at the point marked by blue dot and 1 at the point marked by the red dot at $t = k$. Bottom: outputs from simulations, read at a point on the interior of the domain.

the FD paradigm, one proceeds with a specialised boundary update only when there is a ghost node to be eliminated. In this case, there is no ghost node at the interior corner node, so one might proceed at $\mathbf{x}_0$ with the usual interior update

$$\hat{p}_0^+ = \lambda^2(\hat{p}_1 + \hat{p}_2 + \hat{p}_3 + \hat{p}_4 - 4\hat{p}_0) + 2\hat{p}_0 - \hat{p}_0^- \,. \qquad (40)$$

The first configuration, seen Fig.7a, is the implied geometry when "non-centered" boundary updates are applied at the points adjacent to the corner node ($\mathbf{x}_3$ and $\mathbf{x}_4$). There is no problem with this case as the re-entrant corner cell is a regular interior cell.

The second configuration, seen Fig.7b, requires more consideration. It has been shown that when centered boundary updates are applied at points $\mathbf{x}_3$ and $\mathbf{x}_4$ they correspond to half-cells. Simply applying (40) to the interior corner node [18] would imply that $\mathcal{C}_0$ is no different from an interior cell, but this would not agree with the half-cell neighbours, since the side lengths do not match. A more coherent update at $\mathbf{x}_0$ for this configuration would take into account the volume and sides of this "three-quarter cell". It would be difficult to arrive at such an update using only the FD framework since there are no accessible side and volume parameters to set. On the other hand, the following update, which is consistent with the 90-degree interior corner, can be obtained from a FV perspective:

$$\hat{p}_0^+ = \left(\frac{2\lambda^2}{3} (2\hat{p}_1 + 2\hat{p}_2 + \hat{p}_3 + \hat{p}_4 - 6\hat{p}_0) + 2\hat{p}_0 + \sigma_2 \hat{p}_0^- \right) / \sigma_1 \,, \qquad (41)$$

where $\sigma_1 = 1 + \frac{2\gamma\lambda}{3}$ and $\sigma_2 = \frac{2\gamma\lambda}{3} - 1$. This update ensures stability because $V_0^* = 0$ for the three-quarter cell.

It remains to be seen if the usual update, (40), applied at the interior corner node in the "centered" configuration leads to instabilities. To this end, consider the following experiments on the two L-shaped geometries depicted in Fig. 8. The boundaries are made lossless ($\gamma = 0$) and the usual interior update (40) is applied to the interior corner node. The Courant number is set to the usual $\lambda = \sqrt{1/2}$. The input and output locations are marked in the figures, and the scheme is excited by a non-zero initial condition. The two outputs are shown in Figs. 8a and 8b. In the first case the scheme is clearly unstable as it exhibits exponential growth. However, the same growth is not seen in the second case, even after 3×10^5 time-steps. Thus, employing the usual update at a re-entrant corner adjacent to "centered" boundaries does not always

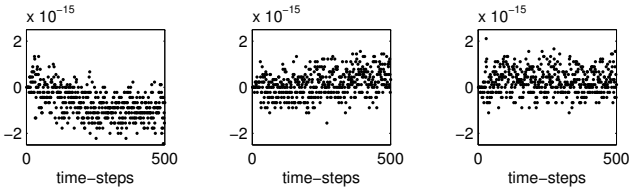

Figure 9: Energy variation for re-entrant corner tests on Domain A using three-quarter cell (left), full cell (middle), and DWM boundaries (right).

lead to instabilities and appears to depend on the overall geometry of the domain. Nevertheless, it would be wise to employ (41) or a full-cell variant since stability will be ensured. The problematic domain (Domain A) was also simulated with the three-quarter cell update (41) and, as expected, this simulation was found to be stable, and more precisely, energy-conserving to machine accuracy, as shown in Fig. 9. The energy was calculated using the expression given in [15] (left out for brevity). Employing the full-cell configuration and the 1-D DWM boundaries on the problematic domain also ensures numerical stability and energy-conservation to machine accuracy. The code used for these simulations will be available at: `http://www2.ph.ed.ac.uk/~s1164563/dafx14`.

7. CONCLUSIONS AND FUTURE WORK

In this study, finite volume equivalences were established for certain FD and DWM schemes for the wave equation and staggered (FDTD) schemes for conservation equations. It was shown that the underlying connection between pointwise FD methods and finite volume methods is a pyramidal decomposition, given certain constraints on the volumetric cells and their neighbours. Additional geometrical interpretations were provided for stability conditions. The "centered" and "non-centered" half-plane boundary updates were shown to be special cases of a FV update. The "1-D" DWM boundary model was shown to have a consistent interpretation in $d > 1$, but that there may be discrepancies with the desired acoustic admittance and domain geometry. Commonly used re-entrant corner updates combined with centered edge conditions in the 2-D Cartesian scheme were shown to have geometrical inconsistencies, leading to unpredictable instabilities. A stable and energy-conserving re-entrant corner update was proposed for the 2-D Cartesian case.

It is straightforward to extend the re-entrant corner analysis to more general schemes in 2-D [39] and 3-D [34], of which the standard Cartesian schemes are special cases. As such, the geometric inconsistencies and possible instabilities reported here extend to proposed re-entrant corner boundary updates for nine-point schemes in 2-D [39] and 27-point schemes in 3-D [34], since the volume and side parameters of re-entrant cells were not taken into account when centered conditions were applied to adjacent cells. Such instabilities have been observed in practice using the proposed interior edge conditions [40]. A matrix eigenvalue analysis of the re-entrant edge in the 3-D SLF scheme can also be found in [41] and conclusions were obtained that are similar to those presented here.

One could proceed and work out the correct re-entrant edge and re-entrant corner updates for the 3-D SLF scheme, to be combined with centered half-plane (half-hyperplane) and quarter-plane terminations, but such boundary updates will still amount to "staircase" boundaries for irregular (curved, slanted) geometries, so they will be no more valid than full-cell staircase boundaries, for which

stability is guaranteed (this was proved in Section 5.2). A FV meshing pre-processing step, successfully implemented, should provide coefficients for all the specialised boundary updates. Strategies for meshing will invariably need to take into account stability conditions, and this will present new challenges.

More generalised impedance boundary models, such as those in [18], which differ in the time-varying components, were not featured, but similar impedance boundary conditions can be found in [15]. The analysis presented here extends to those boundary models, since the condition to bound the total interior energy, (20), does not change as long as the discrete temporal operators are chosen properly and the impedance parameters are non-negative [15].

8. REFERENCES

[1] R. Courant, K. Friedrichs, and H. Lewy, "Über die partiellen differenzengleichungen der mathematischen physik," *Mathematische Annalen*, vol. 100, no. 1, pp. 32–74, 1928.

[2] S. A. van Duyne and J. O. Smith III, "Physical modeling with the 2-D digital waveguide mesh," in *Proc. Int. Computer Music Conf. (ICMC)*, Tokyo, Japan, 1993.

[3] L. Savioja, T. J. Rinne, and T. Takala, "Simulation of room acoustics with a 3-D finite difference mesh," in *Proc. Int. Computer Music Conf. (ICMC)*, Danish Institute of Electroacoustic Music, Denmark, 1994, pp. 463–466.

[4] D. Botteldooren, "Finite-difference time-domain simulation of low-frequency room acoustic problems," *J. Acoustical Society of America*, vol. 98, pp. 3302–3308, 1995.

[5] J. G. Meloney and K. E. Cummings, "Adaptation of FDTD techniques to acoustic modeling," in *11th Annual Review of Progress in Applied Computational Electromagnetics*, vol. 2, 1995, pp. 724–731.

[6] A. Saleh and P. Blanchfield, "Analysis of acoustic radiation patterns of array transducers using the TLM method," *International Journal of Numerical Modelling: Electronic Networks, Devices and Fields*, vol. 3, no. 1, pp. 39–56, 1990.

[7] K. S. Yee, "Numerical solution of initial boundary value problems involving Maxwell's equations in isotropic media," *IEEE Trans. Antennas and Propagation*, vol. 14, no. 3, pp. 302–307, 1966.

[8] P. B. Johns, "Simulation of electromagnetic wave interactions by transmission-line modelling (TLM)," *Wave motion*, vol. 10, no. 5, pp. 597–610, 1988.

[9] A. Taflove, "Application of the finite-difference time-domain method to sinusoidal steady-state electromagnetic-penetration problems," *IEEE Trans. Electromagnetic Compatibility*, vol. EMC-22, no. 3, pp. 191–202, 1980.

[10] S. Bilbao, "Wave and scattering methods for the numerical integration of partial differential equations," Ph.D. thesis, Stanford University, 2001.

[11] G. Cohen, *Higher-order numerical methods for transient wave equations*. Springer-Verlag, 2002.

[12] L. Rhaouti, A. Chaigne, and P. Joly, "Time-domain modeling and numerical simulation of a kettledrum," *J. Acoustical Society of America*, vol. 105, pp. 3545–3562, 1999.

[13] B. Heinrich, "Boundary value problems and irregular networks," in *Finite Difference Methods on Irregular Networks*. Springer, 1987, pp. 17–39.

[14] D. Botteldooren, "Acoustical finite-difference time-domain simulation in a quasi-Cartesian grid," *J. Acoustical Society of America*, vol. 95, pp. 2313–2319, 1994.

[15] S. Bilbao, "Modeling of complex geometries and boundary conditions in finite difference/finite volume time domain room acoustics simulation," *IEEE Trans. Audio, Speech, and Language Processing*, vol. 21, no. 7, pp. 1524–1533, Jul. 2013.

[16] B. Hamilton and C. J. Webb, "Room acoustics modelling using GPU-accelerated finite difference and finite volume methods on a face-centered cubic grid," in *Proc. Digital Audio Effects (DAFx)*, Maynooth, Ireland, Sep. 2013, pp. 336–343.

[17] D. T. Murphy and M. Beeson, "The KW-boundary hybrid digital waveguide mesh for room acoustics applications," *IEEE Trans. Audio, Speech, and Language Processing*, vol. 15, no. 2, pp. 552–564, 2007.

[18] K. Kowalczyk and M. van Walstijn, "Formulation of locally reacting surfaces in FDTD/K-DWM modelling of acoustic spaces," *Acta Acustica united with Acustica*, vol. 94, no. 6, pp. 891–906, 2008.

[19] G. E. Forsythe and W. R. Wasow, *Finite-difference methods for partial differential equations*. New York: Wiley, 1960.

[20] R. M. Alford, K. R. Kelly, and D. M. Boore, "Accuracy of finite-difference modeling of the acoustic wave equation," *Geophysics*, vol. 39, no. 6, pp. 834–842, 1974.

[21] M. A. Dablain, "The application of high-order differencing to the scalar wave equation," *Geophysics*, vol. 51, no. 1, pp. 54–66, 1986.

[22] J. Botts and L. Savioja, "Integrating finite difference schemes for scalar and vector wave equations," in *Proc. IEEE ICASSP*, Vancouver, Canada, 2013, pp. 171–175.

[23] R. D. Richtmyer and K. W. Morton, *Difference methods for initial-value problems*, 2nd ed. Interscience Publishers, 1967, ch. 10: Sound Waves.

[24] G. W. Platzman, "The lattice structure of the finite-difference primitive and vorticity equations," *Monthly Weather Review*, vol. 86, no. 8, pp. 285–292, 1958.

[25] A. Okabe, B. Boots, K. Sugihara, and S. N. Chiu, *Spatial tessellations: concepts and applications of Voronoi diagrams*. John Wiley & Sons, 2009, vol. 501.

[26] S. A. van Duyne and J. O. Smith III, "The 3D tetrahedral digital waveguide mesh with musical applications," in *Proc. Int. Computer Music Conf. (ICMC)*, Hong Kong, 1996, pp. 9–16.

[27] J. Tuomela, "Fourth-order schemes for the wave equation, Maxwell equations, and linearized elastodynamic equations," *Numerical Methods for PDEs*, vol. 10, no. 1, pp. 33–63, 1994.

[28] Y. Liu, "Fourier analysis of numerical algorithms for the Maxwell equations," *J. Comp. Phys.*, vol. 124, no. 2, pp. 396–416, 1996.

[29] J. A. Laird, "The physical modelling of drums using digital waveguides," Ph.D. thesis, University of Bristol, 2001.

[30] M. Kendall, *A Course in the Geometry of n Dimensions*. Hafner, New York, 1961.

[31] L. Kelders, J. F. Allard, and W. Lauriks, "Ultrasonic surface waves above rectangular-groove gratings," *J. Acoustical Society of America*, vol. 103, no. 5, pp. 2730–2733, 1998.

[32] W. J. Karplus, "An electric circuit theory approach to finite difference stability," *Trans. of the AIEE, Part I: Communication and Electronics*, vol. 77, no. 2, pp. 210–213, 1958.

[33] S. Bilbao, *Numerical sound synthesis: finite difference schemes and simulation in musical acoustics*. Wiley, 2009.

[34] K. Kowalczyk and M. van Walstijn, "Room acoustics simulation using 3-D compact explicit FDTD schemes," *IEEE Trans. Audio, Speech, and Language Processing*, vol. 19, no. 1, pp. 34–46, 2011.

[35] J. B. Schneider, C. L. Wagner, and R. J. Kruhlak, "Simple conformal methods for finite-difference time-domain modeling of pressure-release surfaces," *J. Acoustical Society of America*, vol. 104, no. 6, pp. 3219–3226, 1998.

[36] J. G. Tolan and J. B. Schneider, "Locally conformal method for acoustic finite-difference time-domain modeling of rigid surfaces," *J. Acoustical Society of America*, vol. 114, no. 5, pp. 2575–2581, 2003.

[37] J. Häggblad and B. Engquist, "Consistent modeling of boundaries in acoustic finite-difference time-domain simulations," *J. Acoustical Society of America*, vol. 132, no. 3, pp. 1303–1310, 2012.

[38] K. Kowalczyk and M. van Walstijn, "Formulation of a locally reacting wall in finite difference modelling of acoustic spaces," in *Proc. Int. Symp. on Room Acoustics*, 2007, pp. 1–6.

[39] K. Kowalczyk and M. van Walstijn, "Wideband and isotropic room acoustics simulation using 2-D interpolated FDTD schemes," *IEEE Trans. Audio, Speech, and Language Processing*, vol. 18, no. 1, pp. 78–89, 2010.

[40] N. Borrel-Jensen, "Real-time auralisation of the lower frequency sound field using numerical methods on the GPU," M.Sc. thesis, RWTH Aachen University and University of Copenhagen, 2012.

[41] J. Botts and L. Savioja, "Spectral and pseudospectral properties of finite difference models used in audio and room acoustics," *IEEE/ACM Trans. Audio, Speech, and Language Processing*, vol. 22, no. 9, pp. 1403–1412, Sept 2014.